17th World Conference on Earthquake Engineering, 17WCEE
Sendai, Japan - September 13th to 18th 2020

COMPONENT LEVEL SEISMIC FRAGILITY ASSESSMENT OF MULTISPAN CONTINUOUS RC INTEGRAL ABUTMENT BRIDGES

B. F. Ahmed[(1)], K. Dasgupta[(2)]

[(1)] *Ph.D., Indian Institute of Technology Guwahati, India, benazir@iitg.ac.in*
[(2)] *Associate Professor, Indian Institute of Technology, India, kd@iitg.ac.in*

Abstract

The probabilistic approach to assessment of seismic vulnerability for bridges lies in the generation of fragility curves that inherently consider the uncertainties associated with the structural characteristics and the earthquake ground motions. The present study intends to generate component level fragility curves for a class of multispan continuous reinforced concrete integral abutment bridges with dense compacted backfill and elastomeric bearings with dowel bars at the bents. The foundations consist of group of piles symmetrically arranged below the multicolumn bents and single row of piles at the abutments on loose sandy soil.

To account for the uncertainties in the bridge class characteristics, bridge system samples are generated employing Latin Hypercube Sampling technique on the adopted practical ranges of structural and geotechnical properties of the system components. Pile limit states are evaluated by carrying out pushover analysis of the pile-soil system samples considering nonlinear soil-structure interaction. Limit states for the backfill are evaluated considering its mobilised stress-strain behaviour during the movement of the rigid backwall towards it for each of the abutment-backfill system samples. Pier limit states are evaluated by monitoring different possible failure modes during the pushover analyses of the pier samples. Bearing limit states are evaluated by the parallel combination of the pad and the dowel behaviours in the bearing samples. The bridge components and/or the correponding lateral force deformation responses are modeled with appropriate elements using the computer program OpenSees. MDOF capacity spectra for the system samples are generated using displacement based adaptive pushover analysis in OpenSees, wherein, the load vector at each incremental analysis step is updated based on the nonlinear states of the components. Occurrences of component limit states are monitored during the generation of the spectra, which are then converted into the equivalent SDOF spectra. Randomness in earthquake ground motions is incorporated by selecting the motions based on ranges of frequency contents. Probabilistic seismic demand analysis for the bridge class is carried out by pairing each of the system samples with all the ground motions. System demand at each component limit state is obtained by merging the SDOF spectra at that limit state with the demand spectra, reduced for the corresponding system damping. Component-level fragility curves are derived by computing the exceedance probability of each of the component limit states numerically from the corresponding component capacity and demand distributions.

From the results, it is observed that the abutment piles and backfill are seismically the most vulnerable components, while bearing followed by bent pier and pier piles are the least vulnerable ones. Precise fragility estimates are obtained employing the limit states, evaluated by considering soil-structure interaction and various failure modes appropriately, rather than using the defined limit states from the past case-specific studies. Also, the possible overestimation or underestimation owing to rather rough fit or misfit of the evaluated distributions to lognormal model is ruled out by estimating the probabilities numerically, instead of adopting the traditional lognormal fragility formulation. Due to the ability of the adopted adaptive capacity spectrum procedure to track the dynamic characteristic changes, it is expected to yield reliable results with lesser efforts.

Keywords: Seismic fragility, limit states, probability of exceedance, intensity measure, adaptive capacity spectrum.

1. Introduction

Past earthquakes have revealed bridges vulnerable to seismic damages/failures. Assessing a priori the vulnerability of these critical links in a transportation network can aid in effectively carrying out the hazard mitigation operations. Within a probabilistic framework, assessment is done through fragility curve generation, which implies the probabilities of exceedance of an identified Damage State (DS) for varying levels of seismic hazard. The approach, inherently considering the uncertainties associated with structural capacity and demand, is expected to provide reliable vulnerability estimates and thus has become the recent trend, as adopted by studies like [1,2] etc.

This study focuses on generating component level fragility curves of multispan continuous Reinforced Concrete (RC) Integral Abutment (IA) Bridges (IABs), owing to limited fragility studies corresponding to this configuration, e.g., [3,4] among a few and very few in Indian context like [5]. The adopted configuration consists of dense compacted backfill, with the superstructure supported on elastomeric bearings with dowel bars at the multicolumn bents comprising circular piers. Foundations consist of a group (symmetrically arranged) and a single row of RC square piles in loose sand respectively, at each bent and abutment, as in India wherein there is tendency to use RC piles (following their traditional use in non-integral bridges) instead of the typical steel H piles used in countries with expertise in IAs. Such a configuration is shown in Fig. 1(a). Soil Structure Interaction (SSI), being an IAB attribute, only a few studies, e.g., [6, 7] etc. have addressed it in a detailed manner. Hence, this study analyses SSI minutely for Abutment Backfill System (ABS) and Pile Soil System (PSS), so as to evaluate their respective damages precisely. Although, LS prescriptions exist in literature for the adopted components in this study, those correspond to specific properties in the respective studies and hence unsuitable for usage in a different study. Thus, to achieve accurate fragility estimates, component damage models are developed in the study and further employed to obtain LS (quantitative evaluation of DSs) values over ranges of variations of the respective parameters.

2. Seismic Characterisation and Modeling of the Bridge Components

In the study, linear elastic behaviour is expected for the superstructure, abutment backwall, wingwall and cap beam, while bearing, pier, PSS and ABS undergo possible damages. To reflect the possible linear/nonlinear behaviour, modeling is carried out appropriately using the OpenSees software [8].

2.1 Linear elastic components

Superstructure is modeled as a spline (single elastic frame element), with stiffness computed from the material properties, dimensions, and locations of girders and deck sections. Abutment back wall and cap beam are modeled using elastic frame elements, discretised respectively at the underlying pile locations with the central node connected to the spline and at the pier locations with rigid connections with pier top nodes.

2.2 Bearing

Bearing consists of a rubber pad, with two steel dowel bars embedded, as in Fig. 1(b), for longitudinal (L) and transverse (T) directions. Under lateral loading, pad undergoes shear deformation until its force capacity F_{brp} (against coefficient of friction μ_{brp} (calculated using [9]) at the rubber-concrete capbeam interface) is exceeded, after which it is free to slide at F_{brp} (Fig. 1(c)). Each bar of diameter d_{brd} deforms in a cantilever mode, as its steel reaches ultimate flexure stress at the most critical section (adjacent to the interface), resulting in fracture at shear force $F_{u,brd}$ and deformation $d_{u,brd}$ and separation of the cantilever part from embedded portion (Fig. 1(d)). $F_{u,brd}$ is based on a static force applied at height equal to pad thickness h_{br} from interface (considered as fixed). The constituents work in parallel, e.g., with a resisting force $F_{brp} + F_{u,brd}$ (Fig. 1(e)) at the instant of sliding. With the individual Lateral Force Deformation Responses (LFDRs) (Fig. 1(f)), derived numerically for given parameter values, the bearing LFDR is generated (Fig. 1(g)) and modeled using ZeroLength spring element at the bearing location in [8].

2.3 Pier

Bridge pier of height H_{pr} and diameter D_{pr} is assumed to be restrained against rotation at both ends due to rigid connections with the cap beam and the pile cap, leading to its double curvature bending under seismic load F_{pr} (Fig. 1((h)). To derive its LFDR, Displacement based Pushover Analysis (DPoA) with the control node at pier top, following gravity analysis for the imposed axial load P_{pr}, is carried out in [8]. Herein, the pier model is built in, as nonlinearBeamColumn element, with the two end nodes kept fixed against rotation. A typical fibre section, comprising core and cover concrete patches and layer of reinforcing bars, is depicted in Fig. 1(i), with the representative stress-strain curves shown in Figs. 1(j) and 1(k) respectively. Core and cover concretes are modeled using Concrete 06 (computing the confined stress $f_{cc,\,pr}$ for the characteristic compressive stress $f_{ck,\,pr}$ and strain based on pier longitudinal and transverse reinforcement ratios $\rho_{l,\,pr}$ and $\rho_{t,\,pr}$, employing [10]) and Concrete 07 materials respectively. Cold-worked steel bars with yield $f_{y,\,pr}$ and ultimate $f_{u,\,pr}$ stresses and ultimate strain $\varepsilon_{su,\,pr}$ are modeled with Steel02 material.

Using the pier LFDR, the resultant LFDR for the bents with given number of piers is evaluated and modeled using ZeroLength spring element at the pier location in [8].

2.4 Pile-soil system

The fixed head square piles of size D_{pl} and length L_{pl}, founded in the loose sandy with effective friction angle φ_{pl}, belong to the flexible pile category. Hence, under the pile head lateral load F_{pl}, only a certain portion of L_{pl} near the pile cap participates (Fig. 1(l)). The study evaluates Pile Soil Interaction (PSI) through Strain Wedge Model (SWM) [11] which considers a Soil Passive Wedge (SPW) developing at the horizontal soil strain ε_{pl} (uniform throughout SPW), as pile gets displaced laterally towards soil. The configuration of i^{th} SPW, corresponding to the mobilised values ε_{pl_i} and φ_{pl_i} of ε_{pl} and φ_{pl} respectively, is assessed, conditioning on the equilibrium of the soil horizontal stress change at the SPW face and shear stress at the pile-soil interface with the impending pile deflection pattern, for given values of F_{pl_i} and P_{pl} and pile head constraints. To compute p (soil reaction), y (pile deflection, designated as y_{pl} hereafter) and thus the modulus of subgrade reaction E_{pls} profiles along the pile length, SWM discretises L_{pl} and the surrounding soil, into segments and sublayers respectively of equal and constant thickness. At ε_{pl_i}, for soil sublayer j at depth z_j, SWM evaluates p_{ij}, $y_{pl_{ij}}$, $E_{pls_{ij}}$ and the pile head deflection ($y_{0_{pl}}$). As the SWM parameters are being based on an assumed value h_i of SPW depth, accurate estimation requires iterations till the SWM values converge with those obtained by solving the Beam on Winkler Foundation (BWF) equation for the pile under F_{pl_i} and P_{pl}. E_{pls} values below SPW are taken to increase linearly with depth.

Pile is modeled with dispBeamColumn element with similar fibre section details (square section), as in Fig. 1(m), 1(j) and 1(k), based on the pile parameters $f_{ck,pl}$, $f_{cc,pl}$, $f_{y,pl}$, $\rho_{l,pl}$, $\rho_{t,pl}$, as defined for pier. Soil is modeled with ZeroLength spring elements, distributed along the pile length, each having one end connected to a pile node (pile is discretised along its length at the same locations, as done while calculating the SWM parameters) and the other end fixed (Fig. 1(n)). At node j at depth z_j, $E_{pls_{ij}}$ (from SWM at ε_{pl_i}) and $t_j - z_{sf_j}$ values (pile shaft friction - vertical deflection [12], at each j^{th} soil sublayer) are incorporated in the Elastic and ElasticPP (perfectly plastic) uniaxial materials [8] assigned to the j^{th} lateral and vertical element springs respectively. $q - z_{tip}$ values (pile end bearing - tip deflection [12]) are incorporated in the ElasticMultilinear uniaxial material [8] assigned to the vertical spring at the pile tip node.

SWM parameters are computed in spreadsheet and BWF analysis is done in [8] through DPoA of PSS to yield appropriate values for F_{pl_i}, p_i and y_{pl_i} profile. Repeating the procedure for each increasing value of ε_{pl}, leads to $p-y$ curves and pile head LFDR. Precision of the implemented technique is validated through a good agreement of SWM results with those of field static load test [13] (Figs. 1(o) and 1(p)).

Using the pile LFDR, the resultant LFDRs for the foundations with given number of piles respectively below each bent and abutment are evaluated and modeled using ZeroLength spring elements [8].

2.5 Abutment-backfill system

For a typical ABS (Fig. 1(q) for IA in the study), the mobilised Abutment Backfill Interaction becomes a plane-strain problem, as the backwall (with length being much greater than height H_{ab}) is displaced laterally towards the backfill (with friction angle φ_{ab}). Such a model (by [14]) is adopted herein, which considers an intermediately developed i^{th} failure surface (Fig. 1(r)) against the mobilised value SL_{ab_i}, H_{ab,m_i} and φ_{ab,m_i} of the backfill stress level SL_{ab}, H_{ab} and φ_{ab} respectively. Force F_{ab_i} and deformation y_{ab_i} are evaluated, dividing the surface into vertical slices and considering interslice force equilibrium and soil slice shear strain accumulation. LFDR can be evaluated numerically for given ABS parameter values and modeled using ZeroLength spring [8] with one node connected to the backwall central node, the other being fixed.

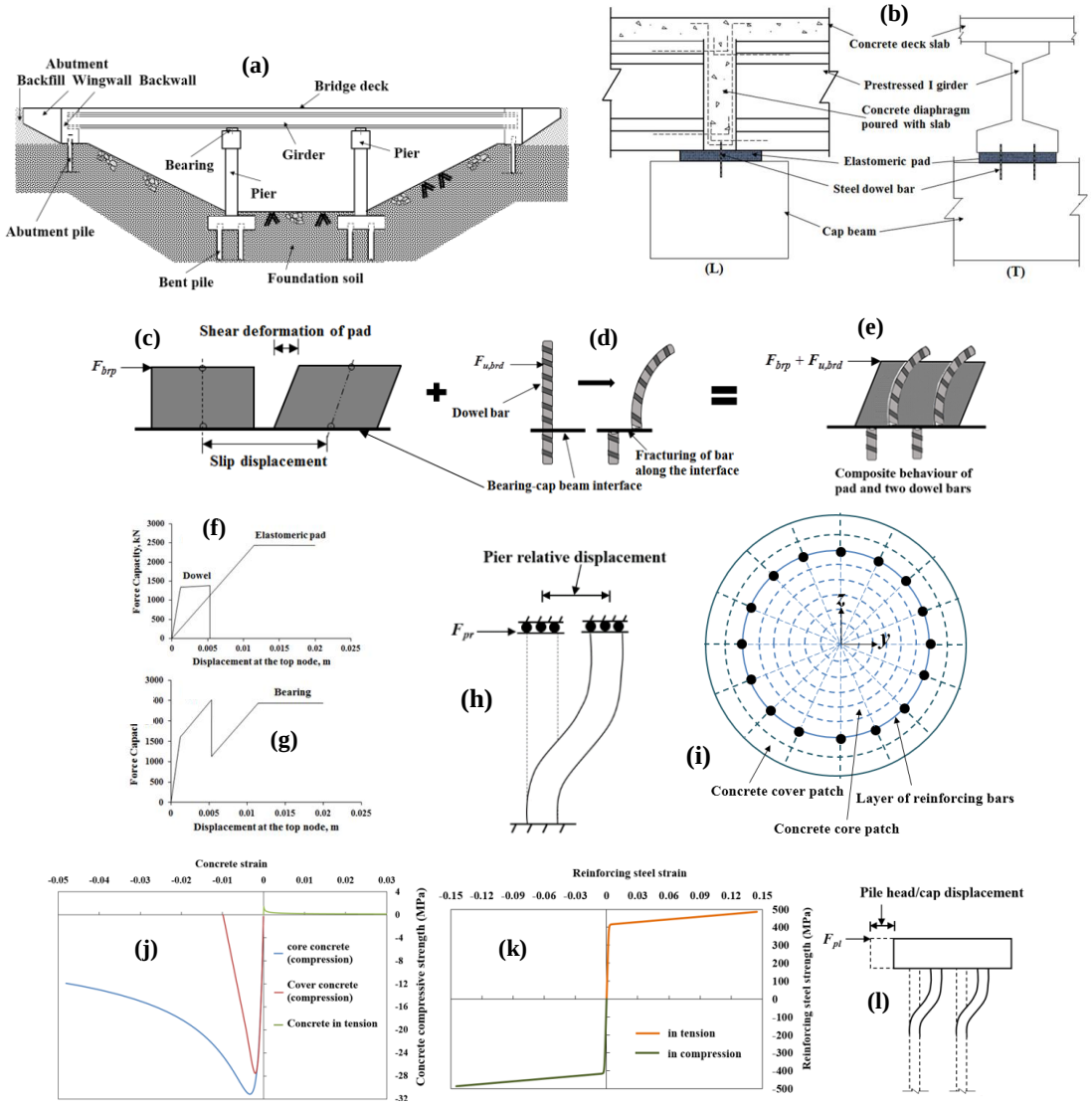

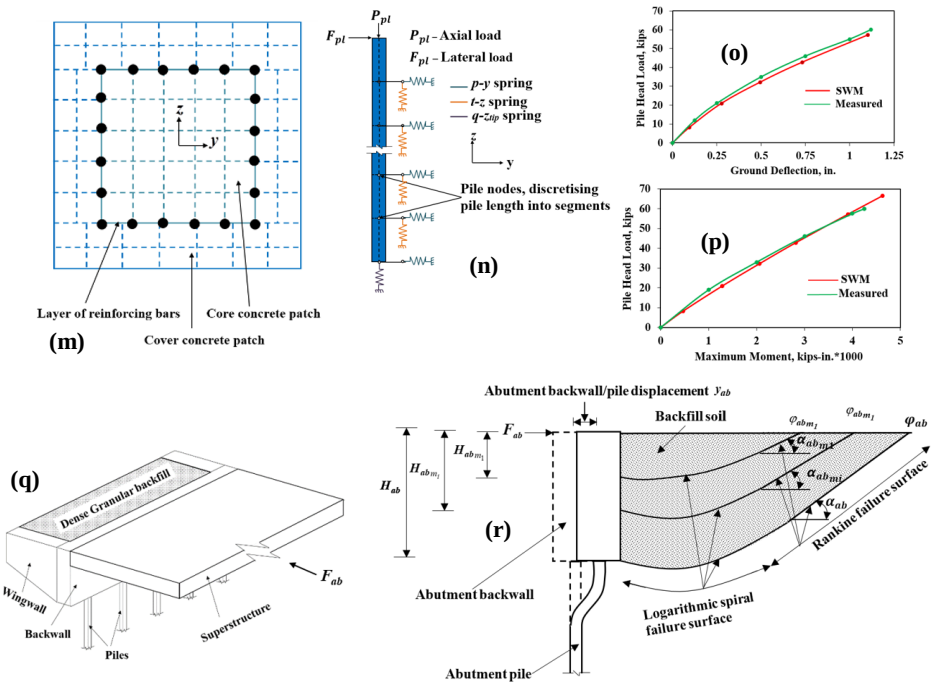

Fig. 1 (a) A typical IAB, (c) bearing arrangement, (c) pad shear deformation, (d) dowel cantilever action, (e) bearing composite action; LFDRs of (f) individual bearing constituents and (g) bearing; (h) pier seismic deformation, (i) pier RC fibre section; sample stress strain curves for (j) concrete and (k) reinforcing steel; (l) pile foundation seismic deformation, (m) pile RC fibre section, (n) BWF model of PSS; comparison of results between SWM and Mustang Island field test for pile head load versus (o) ground deflection and (p) maximum moment; (q) a typical IA and (r) abutment-backfill-foundation seismic deformation.

3. Development of Damage Models

Damage model identifies different damage levels, i.e., DSs for a component, as its LFDR path progresses. DS capacities are quantified as Limit States (LSs) with Limit State Thresholds (LSTs) being the values at the DS onsets, in the same metric as the Engineering Demand Parameters (EDPs) which measure the seismic responses. Pier, bearing, ABS and PSS DSs and LSTs are described in Tables 1, 2, 3 and 4 respectively.

Table 1 – Damage state definitions and limit state thresholds adopted for pier.

Damage states	Limit state thresholds	
	From flexural analysis	Adopted
Slight – fully operational	$d_{1,pr_f} : \varepsilon_{s,pr} = \varepsilon_{sy,pr}$	$\mu_{d_{1,pr}} : \min(\mu_{d_{1,pr_f}}, \mu_{d_{1,pr_s}}, \mu_{d,pr_\delta}, \mu_{d,pr_b})$
Moderate- repairable damage, limited service	$d_{2,pr_f} : \min\begin{pmatrix} d_{pr} : \varepsilon_{c,pr} = 0.004 \\ d_{pr} : \varepsilon_{s,pr} = 0.015 \end{pmatrix}$	$\mu_{d_{2,pr}} : \min(\mu_{d_{2,pr_f}}, \mu_{d_{1,pr_s}}, \mu_{d,pr_\delta}, \mu_{d,pr_b})$
Extensive – Significant damage	$d_{3,pr_f} : \varepsilon_{cu,pr} = 0.004 + \frac{1.4\rho_{t.pr}\varepsilon_{su,pr} f_{y,pr}}{f_{cc,pr}}$	$\mu_{d_{3,pr}} : \min(\mu_{d_{3,pr_f}}, \mu_{d_{1,pr_s}}, \mu_{d,pr_\delta}, \mu_{d,pr_b})$
Collapse Prevention	$d_{4,pr_f} : \min\begin{pmatrix} d_{pr} : M_{pr} \le 0.85 M_{pr\max} \\ d_{pr} : \varepsilon_{s,pr} = 0.75\varepsilon_{su,pr} \end{pmatrix}$	$\mu_{d_{4,pr}} : \min(\mu_{d_{4,pr_f}}, \mu_{d_{1,pr_s}}, \mu_{d,pr_\delta}, \mu_{d,pr_b})$

where, d_{i,pr_f} = relative displacement of pier top in flexure (i = 1 to 4), $\mu_{d_{i,pr}}$ = displacement ductility, with suffices f, s, δ and b respectively against flexure, shear, P-delta effect and buckling, $\varepsilon_{sy,pr}$ = yield value of strain $\varepsilon_{s,pr}$ in steel extreme fibre, $\varepsilon_{cu,pr}$ = compressive strain in concrete extreme fibre against fracture of

transverse reinforcement, M_{pr} is the bending moment with the maximum value $M_{pr\max}$ in pier.

Table 2 – Damage state definitions and limit state thresholds adopted for bearing.

Damage State	Limit State Thresholds
Slight – dowel fracture, bridge in full operation, some degree of repair and deck realignment	$d_{1,br} : d_{u,brd}$
Moderate- onset of sliding, 50% service disruption	$d_{2,br}$: either $\begin{pmatrix} d_{brp}\,(\text{if} > d_{u,brd}) \\ d_{u,brd}\,(\text{if} > d_{brp}) \end{pmatrix}$
Extensive – Limited to emergency traffic	$d_{3,br} : d_{sl,br} = W_{seat}/2$
Collapse Prevention	$d_{4,br} : d_{sl,br} = W_{seat}$ (seat width)

where, $d_{i,br}$ = bearing displacement (i = 1 to 4), d_{brp} = pad shear deformation, $d_{sl,br}$ = sliding displacement.

For most bearing samples, dowel fracture occurs much earlier to pad reaching F_{brp}, leading to bearing sliding. For a few samples (with high dowel bar stiffness), second DS is not just characterised by F_{brp}, as sliding for such samples is restricted by the dowels in place, with its fracture occurring much after the attainment of F_{brp}. For such a sample, LSTs with respect to both the DSs are taken to that at the fracture.

Table 3 – Damage state definitions and limit state thresholds adopted for ABS.

Damage State				Limit State Thresholds
Abutment-backfill system (in the study)	Bridge system level	Component-level (References) [3]	Component-level (References) [15]	
Slight - repairable minor functional damage	Slight	$0.1\,y_{ab_{\max}}$ -moderate	$0.35\,y_{ab_{\max}}$ - extensive	$d_{1,ab} : SL_{ab} = 80\%$
Extensive - significant reduction in shear modulus of sandy backfill; repairable major functional damage	Moderate	$0.35\,y_{ab_{\max}}$ - extensive	$y_{ab_{\max}}$ -ultimate	$d_{2,ab} : SL_{ab} = 95\%$
Ultimate - zero lateral stiffness, replacement needed	Extensive	$y_{ab_{\max}}$ -ultimate	-	$d_{2,ab} : SL_{ab} = 100\%$

where, $d_{i,ab}$ = LST values in terms of y_{ab} (i^{th} DS rank, i = 1 to 3), $y_{ab_{\max}}$ = backfill maximum displacement capacity. ABS sample analyses reveal $0.1\,y_{ab_{\max}}$ and $0.35\,y_{ab_{\max}}$ to be approximately equal to y_{ab} s at $0.72\,SL_{ab}$ and $0.90\,SL_{ab}$ respectively in the study, attaining $y_{ab_{\max}}$ at $1\,SL_{ab}$.

Table 4 – Damage state definitions and limit state thresholds adopted for PSS.

Damage State	Limit State Thresholds
Serviceable - elastic behaviour ends, minor functional damage	$d_{1,pl} : \varepsilon_{s,pl} = \varepsilon_{sy,pl}$
Ultimate- unrepairable major damage, component replacement.	$d_{2,pl} : \varepsilon_{cu,pl} = 0.004 + \dfrac{1.4\rho_{t,pl}\varepsilon_{su,pl} f_{y,pl}}{f_{cc,pl}}$

where, $d_{i,pl}$ = pile head displacement (i = 1 to 2), $\varepsilon_{sy,pl}$ and $\varepsilon_{su,pl}$ = yield and ultimate values respectively.

Table 4 – Damage state definitions and limit state thresholds adopted for PSS.

Damage State	Limit State Thresholds
Serviceable - elastic behaviour ends, minor functional damage	$d_{1,pl} : \varepsilon_{s,pl} = \varepsilon_{sy,pl}$
Ultimate- unrepairable major damage, component replacement.	$d_{2,pl} : \varepsilon_{cu,pl} = 0.004 + \frac{1.4\rho_{t,pl}\varepsilon_{su,pl} f_{y,pl}}{f_{cc,pl}}$

where, $d_{i,pl}$ = pile head displacement (i = 1 to 2), $\varepsilon_{sy,pl}$ and $\varepsilon_{su,pl}$ = yield and ultimate values respectively of $\varepsilon_{s,pl}$, $\varepsilon_{cu,pl} = \varepsilon_{c,pl}$ corresponding to fracture of transverse reinforcement in pile (as in pier).

Damage model analyses of PSS samples (Section 4.2) show no fixed sequence between the Flow Around Failure (FAF) initiation in sand with d_{pl_1} and d_{pl_2}. Hence, PSS DSs are based on pile LSs only. Though FAF is not considered as a DS, it is monitored for modeling its effects on d_{pl_1} and d_{pl_2}.

4. Uncertainty Treatment in Fragility Formulation

Formulation of fragility involves identifying the bridge structural and geotechnical component parameters, affecting the respective capacities (LSTs) as well as demands (EDPs) and thereby modeling the uncertainties. Additionally, demand is significantly influenced by the variation in Ground Motion (GM) characteristics.

As a first step, screening for influential component parameters is carried out through 'One Factor at A Time' approach to sensitivity analysis and the respective sensitivity indices are evaluated to sort out those parameters required to be employed for fragility formulation. Investigation reveals D_{pl}, $f_{ck,pl}$, $f_{y,pl}$, $\rho_{l,pl}$, $\rho_{t,pl}$ and ν_{pl} to be influencing pile LSTs and FAF, while ABS LSTs are affected by H_{ab}, φ_{ab} and $\delta_{f,ab}$ (abutment-backfill interface friction angle δ_{ab}, as a factor of φ_{ab}, varying independently of φ_{ab}). For pier LSTs, H_{pr}, D_{pr}, $\rho_{l,pr}$, $\rho_{t,pr}$, $f_{ck,pr}$, $f_{y,pr}$, υ_{pr} are found as significant. h_{br}, d_{brd} and $\varepsilon_{su,brd}$ (dowel steel ultimate strain), G (pad shear modulus) and σ_m (bearing normal stress) for bearing initial LSTs.

4.1 Uncertainty modeling of bridge sensitive parameters and ground motions

Component parameters influencing the respective LSTs are modeled as random variables with certain probability distributions, either assumed or adopted from literature (Table 5), where l, u, μ, σ, ν correspond to the upper limit, lower limit, mean, standard deviation, coefficient of variation of the distributions. Geometric variations of superstructure and abutment are also considered (not shown herein) as pier and pile tributary loads are influenced by their weights. GMs to be inputted are selected based on Peak Ground Acceleration(PGA)/Peak Ground Velocity (PGV) (a/v) criterion (high (h), medium (m), low (l) frequency contents) (Table 5, which also lists the spectral acceleration S_a at structural time period of 0.7 secs, i.e., $S_a(0.7s)$), known to encompass wide ranges of earthquakes and thus the possible EDP bounds.

Variation of L_{pl} (though insensitive) is required for mobilising sand axial load capacity adequately to (a) sustain the varying superimposed load and (b) satisfy pile settlement criterion in loose sand.

Table 5 – Probability distribution characteristics for IAB parameters and ground motion variations.

Parameter	Distribution type and properties			Remarks
D_{pr} (m)	Uniform	l = 0.8	u = 2	[16] (slightly relaxed)
H_{pr} (m)	Uniform	l = 5	u = 15	pier aspect ratio range of 2.50 – 18.75
D_{pl} (m)	Uniform	l = 0.35	u = 0.80	[17] (l), Assumed (u)
L_{pl} (m)	Uniform	l =10	u = 15	flexible pile category criteria

h_{br}	Uniform	l = 0.020	u = 0.150	[18]
d_{brd} (m)	Uniform	l = 0.25	u = 0.40	[19] (l), maximum practical value (u)
H_{ab} (m)	Uniform	l = 2	u = 5	[20]
f_{ck} (MPa)	Uniform	l = M25	u = M45	[21] (l), [22] (u)
M25	Normal	μ = 33.75	σ = 5.30	[23]
M45		μ = 56.55	σ = 7.00	
f_y (MPa)	Normal	μ = 509.8	σ = 43.00	[24]
f_u (MPa)		μ = 620.68	σ = 43.61	
ε_{su}		μ and l = 0.145	ν =0.173	[25]
G (MPa)	Uniform	l = 0.80	u = 1.20	[18]
φ_{pl} (°)	Uniform	l = 27	u = 35	[26]
φ_{ab} (°)		l = 35	u = 45	
$\delta_{f,ab}$	Uniform	l = 0.6	u = 0.8	[14]
A_l (%)	Uniform	l = 0.8	u = 4	[22]
s_t (m)		l = 0.08	u = 0.30	

Earthquake	a/v (gs/m)	$S_a(0.7s)$ (g)	Earthquake	a/v (gs/m)	$S_a(0.7s)$ (g)
Loma Prieta (l)	0.490	0.763	Loma Prieta (m)	0.995	0.534
Loma Prieta (l)	0.592	0.697	Chi-Chi (h)	1.839	0.689
Northridge (l)	0.779	0.825	Northridge (h)	2.112	0.528
Petrolia (l)	0.740	1.834	Northridge (h)	1.616	1.850
			Petrolia (h)	2.565	0.275

Parameters are suffixed with '*pr*', '*pl*', '*d*', corresponding to pier, pile and dowel respectively. A_l is the amount of longitudinal reinforcement expressed as percentage of pier gross sectional area.

4.2 Evaluation of probabilistic capacity and demand

To yield capacities and demands in probabilistic terms, BS samples are generated, employing Latin Hypercube Sampling Technique. Firstly, 12 samples are created using the geometric parameter ranges of Table 5; at level 2, 12 sub-samples are generated with the remaining parameter ranges. Linking all the sub-samples to each sample, results in 144 BS models.

Damage model analyses result in dispersed data (144 values) for LST against each component DS, distribution properties of which are listed in terms of μ and ν as well as the median (θ) and dispersion (β) of the transformed (logarithmic) data in Table 6. Data for all components follow lognormal distribution roughly, (as in Fig. 2(a) for pile 1st DS) while ABS follows uniform distribution.

Table 6 – LST distribution properties corresponding to pile, pier, bearing and ABS DSs.

Bridge component LSs		μ	ν	θ	β
Pier	$\mu_{1,pr}$	0.941	0.159	0.924	0.210
	$\mu_{2,pr}$	1.551	0.358	1.427	0.446
	$\mu_{3,pr}$	2.785	0.526	2.311	0.690
	$\mu_{4,pr}$	4.081	0.761	2.945	0.887
Pile (mm)	$d_{1,pl}$	32	0.289	31	0.306
	$d_{2,pl}$	57	0.397	54	0.364

Bearing (m)	$d_{1,br}$		0.019	1.152	0.011	1.094
	$d_{2,br}$		0.043	0.565	0.0370	0.541
	$d_{3,br}$	L	0.331	0.278	0.318	0.292
		T	0.225	0.504	0.195	0.561
	$d_{4,br}$	L	0.662	0.278	0.636	0.292
		T	0.451	0504	0.390	0.561
ABS (mm)	$d_{1,ab}$		27	0.331	26	0.352
	$d_{2,ab}$		90	0.329	85	0.352
	$d_{3,ab}$		163	0.333	153	0.355

Probabilistic seismic demand analysis is carried out through the Inverse Application of Adaptive Capacity Spectrum (IACSM) [27], which employs Displacement based Adaptive Pushover analysis (DAP) on each BS sample. BS model is created in [8] using Structural Components Modeling (SCM) analogy [28] (Fig. 2b), with the automated DAP algorithm [29] (which updates the displacement vector to be imposed to the appropriate nodes of BS at each analysis step k) embedded. The generated MDOF capacity curve is converted into equivalent SDOF Adaptive Capacity Spectrum (ACS), employing the horizontal displacements and the participating masses of all the components as well as the BS base shear at the k^{th} step. The component LSs are monitored along the ACS path. 5% damped Acceleration Displacement Response Spectra (ADRS) are generated for the GMs and reduced for the evaluated resultant BS damping at each component LS, which is the Seismic Demand Spectrum (SDS). ACS is merged with SDS at the LS to obtain the BS spectral acceleration demand $S_{a,D_{BS}}$. Probabilistic Seismic Demand Models (PSDMs), relating the GM Intensity Measure (IM) (PGA and $S_a(0.7s)$ in the study) with the mean Seismic Demands (SDs) placed on the components in terms of the respective EDPs, are developed. $0.7s$ is selected as the average value of the structural nonlinear time period, as it ranges from 0.45 to 1.3 secs from the damage initiation till collapse for BS samples. Component SD distributions and PSDMs are discussed below:

- Pairing up of each of N (=144) nos. of BS analytical models (denoted by BSM_j, $j = 1,2,....N$) with all M (=9) nos. of chosen GMs (denoted by GM_l, $l = 1,2,....M$) to obtain 1296 BSM_j - GM_l pairs.
- Selection of a range R (0.02g to 2g) for PGA as well as $S_a(0.7s)$ (denoted by $IM_{r,PGA}$ and $IM_{r,S_a(0.7s)}$, $r = 1,2,....R$) and thus, scaling up and down each of the GMs from its respective PGA and $S_a(0.7s)$ values to $IM_{r,PGA}$ s and $IM_{r,S_a(0.7s)}$ s respectively.
- IACSM analysis of BSM_j - GM_l pairs, resulting in $(j \times l)$ nos. of $S_{a,D_{BS}}$ values for the i^{th} DS for the p^{th} component at each $IM_{r,PGA}$ / $IM_{r,S_a(0.7s)}$, further converted to displacement demands $S_{d,D_{BS}}$.
- Conversion of $S_{d,D_{BS}}$ s to SD against i^{th} DS of p^{th} component, i.e., $D_{i,p}$ s in terms of its EDP (displacement based in the study), based on mode shape displacement contribution of p^{th} component to the BS equivalent SDOF displacement $S_{d,C_{BS}}$ (from DAP). $D_{i,p}$ data (1296 values) represents a stripe.
- Repetition of above steps over range results in dispersed data ($(i \times j) \times r$) $D_{i,p}$ values. Regressing the data against IM results in PSDM, as in Fig. 2(c) for pile 2nd (i = 2) DS with $D_{2,pl_{mean}}$ as its mean SD.

The above steps are repeated to obtain the SD data at all DSs for every component. EDP data against all the component DSs very roughly follow lognormal distribution, as shown in Fig. 2(d) for bearing 2nd DS.

5. Generation of Component-level Fragility Curves

Seismic fragility can be obtained by the traditional lognormal formulation. However, in the study, neither the

capacities nor demands truly follow lognormal distribution, with ABS uniform capacity distribution as the perfect misfit. Hence, fragilities are evaluated numerically comparing the capacity and demand from each bin and summing up for all events where the capacity is of a particular value (corresponding to a bin) and the demand (bin values) exceeds that capacity value. Fragility curves for PSS, ABS, pier and bearing are shown in Figs. 3(a), 3(b), 3(c) and 3(d) when considering PGA as IM. Also, Fig. 3(a) shows the difference between fragility values obtained numerically and using the traditional formulation.

Not all the 144 bridge cases lead to bearing DSs, as in those cases, pier DSs precede all/a few bearing DSs leading to BS collapse. Also, there are cases where bearing sliding occurs before all/a few pier DSs, leading to collapse. As such, Occurrence Probability (OP) of a bearing/pier DS is calculated as the ratio of the number of damage cases n_i to the total simulation cases N (=144). Probability of exceedance of each DS is obtained by multiplying OP with the probability of exceedance for those samples where it occurs.

Though, not all the bearing samples undergo damages, however in many of those samples showing damages, the first and second DSs precede earlier than the first DS of each of PSS and ABS. This may be the possible reason that the upto certain range of PGA, bearing is more fragile to the initial DSs than PSS and ABS. While demand distributions show high dispersion ($\beta_{D,PGA}$) considering PGA, the corresponding value β_{D,S_a} using $S_a(0.7s)$ is much less, e.g., $\beta_{D,PGA}$ values of 0.719, 0.707 reduce to β_{D,S_a} values of 0.275 and 0.304 respectively for the two PSS DSs. Similarly, $\beta_{D,PGA}$ s of 0.737, 0.750 and 0.778 reduce to β_{D,S_a} s of 0.374, 0.380 and 0.430 for the three ABS DSs respectively. Hence, fragility curves, are evaluated against $S_a(0.7s)$ for PSS and ABS (found to be most vulnerable against PGA) and displayed in Figs. 3(e) and 3(f).

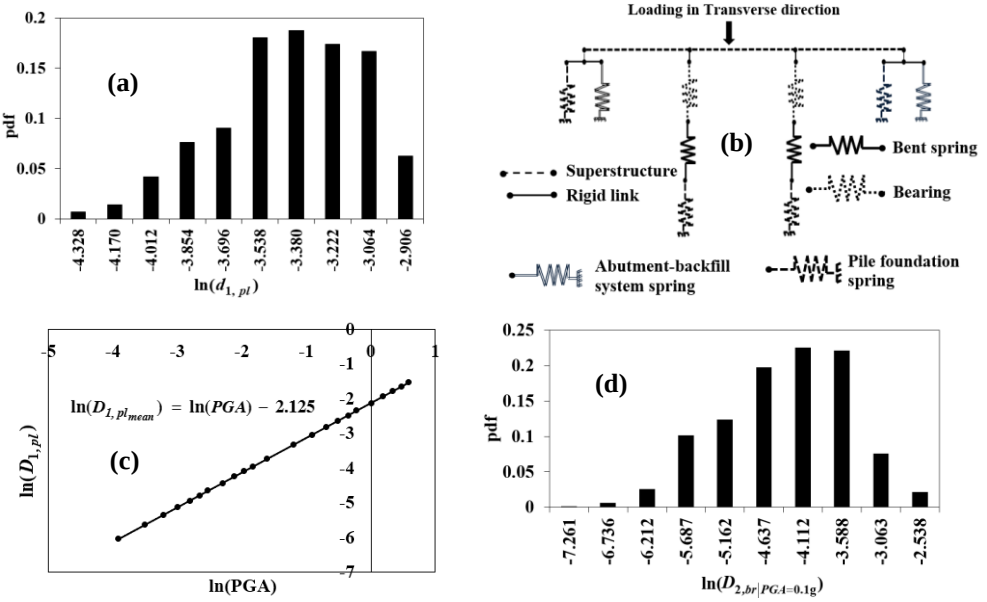

Fig. 2 (a) LST probability distribution obtained for pile 2nd DS, (b) structural component modeling analogy for BS, (c) PSDM corresponding to pile 2nd DS and (c) EDP distribution obtained for bearing 2nd DS.

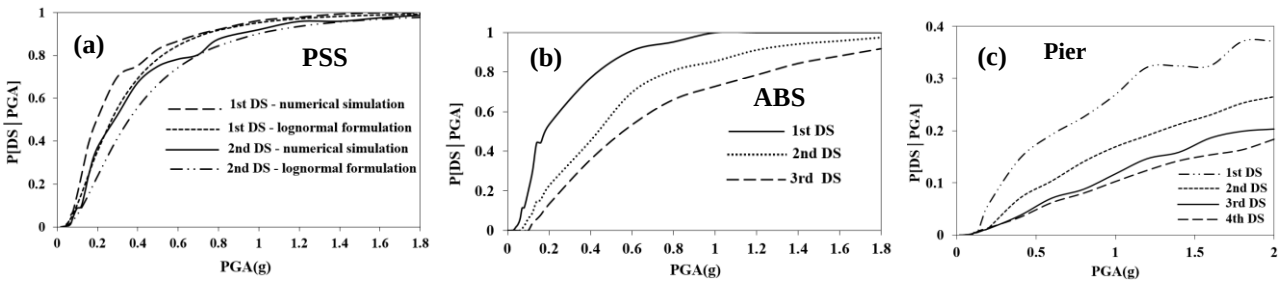

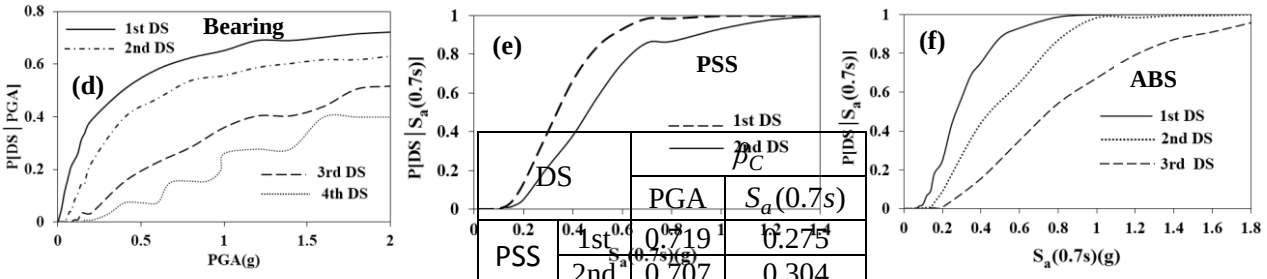

DS		β_C	
		PGA	$S_a(0.7s)$
PSS	1st	0.719	0.275
	2nd	0.707	0.304
ABS	1st	0.727	0.374
	2nd	0.750	0.380
	3rd	0.778	0.430

Fig. 3 Component-level fragility curves evaluated for the IAB configuration in the study.

8. Conclusions

This study attempts to evaluate the vulnerability of IABs, as the assessment corresponding to this class is scanty in the literature and a probabilistic scheme is adopted, since neither the structural capacity nor the demand is deterministic. Conclusions regarding the methodology and the outcomes from the study are:

- Component damage models are developed incorporating multiple failure modes and SSI (being a basic IAB attribute), thus possible overestimation or underestimation of LSTs while considering a single failure mode or ignoring/simplifying SSI is avoided.
- Since LSTs are themselves evaluated in the study, instead of using case specific values from the literature, precise bounds of the expected fragility estimates are expected for the component parameter ranges for the IAB class than adopting values from the literature. It is also justified through the evaluated dispersion in LST values owing to the variation in parameter values.
- The study has employed IACSM for assessing the seismic demand, as it is easier, practically oriented procedure, avoiding the complexities of nonlinear dynamic analyses. However, the accuracy is considered to be at par, as the bridge dynamic characteristics are updated at every step during the entire range of its nonlinear behaviour using the displacement based adaptive algorithm.
- For IAB configuration, the abutment piles as well as the abutment backfill system are the most vulnerable components, as those are the ones to get immediately mobilised in action in resisting the seismic displacements. Bearing, followed by pier and bent piles, are the least vulnerable components.
- For the IAB configuration, spectral acceleration is found to be the better IM than PGA. However, for pier DSs occurring at higher time periods, the dispersion values are found to be the same, indicating equal applicability of both the IMs.

7. References

[1] Nielson, B. G. (2005): Analytical Fragility Curves for Highway Bridges in Moderate Seismic Zones," Ph.D. Thesis, School of Civil and Environmental Engineering, Georgia Institute of Technology.

[2] Ramanathan, K. N., DesRoches, R. and Padgett, J. E. (2012). "A comparison of pre- and post-seismic design considerations in moderate seismic zones through the fragility assessment of multispan bridge classes." *Engineering Structures*, 45, 559–573.

[3] Zakeri B, Padgett JE, Amiri GG (2014): Fragility analysis of skewed single-frame concrete box-girder bridges. *Journal of Performance of Constructed Facilities*, **28** (3), 571-582.

[4] Choine, M. N., O'Connor, A. J. and Padgett, J. E. (2015) "Comparison between the Seismic Performance of Integral and Jointed Concrete Bridges." *Journal of Earthquake Engineering*, 19, 172-191.

[5] Parool, N. and Rai, D. C. (2015). "Seismic fragility of multispan simply supported bridge with drop spans and steel bearings." *Journal of Bridge Engineering*, 20(12), 04015021-11.

[6] Bradley, B. A., Cubrinovski, M., Dhakal, R. P. and MacRae, G. A. (2010). "Probabilistic seismic performance and loss assessment of a bridge–foundation–soil system." *Soil Dynamics and Earthquake Engineering*, 30(5), 395-411.

[7] Padgett, J. E., Ghosh, J., Duenas-Osorio, L. (2013) "Effects of liquefiable soil and bridge modeling parameters on the seismic reliability of critical structural components." *Structure and Infrastructure Engineering*, 9(1), 59-77.

[8] McKenna F, Fenves, GL, Scott MH (2000): Open System for Earthquake Engineering Simulation. *OpenSees Command Manual*. University of California, Berkeley, California.

[9] Schrage, I. (1981). "Anchoring of Bearings by Friction." *Joint Sealing and Bearing Systems for Concrete Structures", World Congress on Joints and Bearings*, 1, Niagara Falls, NY, American Concrete Institute.

[10] Mander JB, Priestley MJ, Park R (1988): Theoretical stress - strain model for confined concrete. *ASCE Journal of Structural Engineering*, **114** (8), 1804-1826.

[11] Ashour M, Norris G (2000): Modeling lateral soil - pile response based on soil-pile interaction. *ASCE Journal of Geotechnical & Geoenvironmental Engineering*, **126** (5), 420–428.

[12] API (2002): Recommended Practice 2A - WSD - Planning, Designing, and Constructing Fixed Offshore Platforms Working Stress Design. American Petroleum Institute, 61-65.

[13] Reese LC, Cox WR, Koop FD (1970). Analysis of laterally loaded piles in sand. *Proc 6th conference of Offshore Technology*, Houston, Texas, paper no. 2080, 473–483.

[14] Shamsabadi A, Ashour M, Norris G (2005): Bridge Abutment Nonlinear Force-Displacement Capacity Prediction for Seismic Design. *ASCE Journal of Geotechnical & Geoenvironmental Engineering*, **131**(2), 151-161.

[15] Choine MN, O'Connor AJ, Padgett JE (2015): Comparison between the Seismic Performance of Integral and Jointed Concrete Bridges. *Journal of Earthquake Engineering*, **19**, 172-191.

[16] Ramanathan KN (2012): Next generation seismic fragility curves for California bridges incorporating the evolution in seismic design philosophy. *Ph.D. Dissertation*, Civil and Environmental Engineering Department, Georgia Institute of Technology.

[17] Hwang H., Liu JB, Chiu Y (2001) Seismic Fragility Analysis of Highway Bridges. Technical Report, MAECRR-4

[18] IRC (1987) Standard Specifications and Code of Practice for Road Bridges, Section IX Bearing, IRC 83-Part II Elastomeric Bearings. Indian Road Congress, New Delhi, India.

[19] IRC (2014b). Guidelines for Design and Construction of Cement Concrete Pavements for Low Volume Road, IRC SP 62. Indian Road Congress, New Delhi, India.

[20] Paraschos A (2016) Effects of Wingwall Configurations on the Behaviour of Integral Abutment Bridges. *Ph.D. Dissertation*, Civil Engineering Department, University of Maryland, College Park, Maryland.

[21] BIS (2010). Design and Construction of Pile Foundations –Code of Practice, Part 1 Concrete Piles Section 1 Driven Cast In-Situ Concrete Piles, IS-2911-Part 1/Sec 1. Bureau of Indian Standards, New Delhi, India.

[22] BIS (2000). Plain and Reinforced Concrete-Code of practice, IS-456. Bureau of Indian Standards, New Delhi, India.

[23] BIS (2009). Indian standard for concrete mix proportioning, IS-10262. Bureau of Indian Standards, New Delhi, India.

[24] Basu PC, Shyiamoni P, Roshan AD (2004): Characterization of steel reinforcement for RC structures: An overview and related issues. *Indian Concrete Journal*, **78** (1), 19-30.

[25] Firat FK (2016): Mechanical Properties of Reinforcing Steel in R/C: Uncertainty Analysis and Proposal of a New Material Factor. *Arabian Journal for Science and Engineering*, **41**(10), 4019-4028.

[26] Laboratory 8. Relative Density and Load Carrying Capacity of Sands. eng.mu.edu/newmand/CEEN%203160%20 Lab8%20RelativeDesnity.pdf. Accessed 24 2017.

[27] Kappos AJ, Saiidi MS, Aydinoglu MN, Isakovic T (2012): *Seismic Design Assessment of Bridges, Inelastic Methods of Analysis and Case Studies*. Geotechnical, Geological and Earthquake Engineering @ Springer.

[28] Priestley MJN, Seible F, Calvi GM (1996): *Seismic Design and Retrofit of Bridges*. John Wiley and Sons, New York.

[29] Antoniou S, Pinho R. (2004): Development and Verification of a Displacement Based Adaptive Pushover Procedure. *Journal of Earthquake Engineering*, **8**(5), 643-661.

